# Augmenting Synthetic Aperture Radar with Space Time Adaptive Processing

Michael Riedl, Lee C. Potter, Emre Ertin

Department of Electrical and Computer Engineering
The Ohio State University, Columbus, OH

## ABSTRACT

Wide-area persistent radar video offers the ability to track moving targets. A shortcoming of the current technology is an inability to maintain track when Doppler shift places moving target returns co-located with strong clutter. Further, the high down-link data rate required for wide-area imaging presents a stringent system bottleneck. We present a multi-channel approach to augment the synthetic aperture radar (SAR) modality with space time adaptive processing (STAP) while constraining the down-link data rate to that of a single antenna SAR system. To this end, we adopt a multiple transmit, single receive (MISO) architecture. A frequency division design for orthogonal transmit waveforms is presented; the approach maintains coherence on clutter, achieves the maximal unaliased band of radial velocities, retains full resolution SAR images, and requires no increase in receiver data rate vis-a-vis the wide-area SAR modality. For $N_T$ transmit antennas and $N$ samples per pulse, the enhanced sensing provides a STAP capability with $N_T$ times larger range bins than the SAR mode, at the cost of $O(\log N)$ more computations per pulse. The proposed MISO system and the associated signal processing are detailed, and the approach is numerically demonstrated via simulation of an airborne X-band system.

**Keywords:** Synthetic aperture radar, Space time adaptive processing, MISO radar

## 1. INTRODUCTION

This paper presents a framework for a multi-input, single-output (MISO) joint synthetic aperture radar (SAR) and space time adaptive processing (STAP) system. Wide- area persistent radar imaging generates large amounts of data that must typically be transmitted and stored. Adding additional receivers typically required for STAP increases the data rate proportional to the number of receivers. To constrain the growth of the data rate, the proposed system utilizes a single receive channel and multiple transmitters to provide the degrees of freedom required for ground moving target indicator (GMTI).

A MISO system requires the use of orthogonal waveforms to separate the channels at the receiver. This paper will use the orthogonal scheme of frequency division multiple access (FDMA) as a point design. Each transmit channel uses linear frequency modulated (LFM) waveforms with a unique carrier frequency to form orthogonal sub-bands. Using this proposed scheme, MISO SAR extensions are discussed to form full-resolution images. Additionally, extensions are derived for FDMA space time adaptive processing. Finally, a wide area radar simulation is presented for quantitative evaluation of this FDMA MISO scheme.

## 2. MISO FDMA CHIRP WAVEFORMS

This proposed FDMA scheme must transmit orthogonal waveforms so that they can be separated at the receiver. Using the traditional LFM waveform, orthogonal waveforms can be achieved using disjoint sub-bands. The $n^{th}$ antenna will then transmit the following LFM waveform at the $m^{th}$ pulse:

$$s_{n,m}(t) = \exp\{j\pi\alpha t^2\}\exp\{j2\pi(f_c + f_{n,m})t\}, \quad -\frac{T}{2} < t < \frac{T}{2}, \quad n = 0, 1, ..., N-1, \quad m = 0, 1, ..., M-1 \ , \quad (1)$$

where $\alpha$, $(f_c + f_{n,m})$, $T$, $N$, and $M$ are the LFM rate, $n^{th}$ sub-band carrier at the $m^{th}$ pulse, pulse duration, number of antennas, and number of pulses respectively. In keeping with this definition and antenna numbering system, the carrier offset for each antenna is calculated as

$$f_{n,m} = \frac{2I_{n,m} - N - 1}{2}\left(\frac{BW}{N}\right) \ , \quad (2)$$

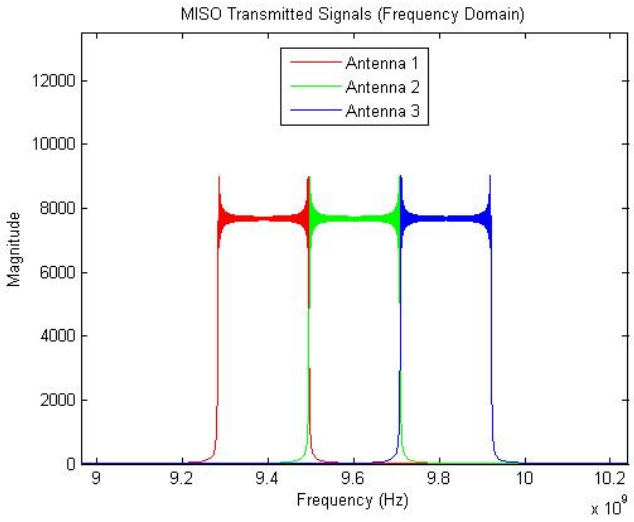


Figure 1: Frequency spectrum for transmitted waveforms.

where $I_{n,m}$ is an indexing variable we will define in Section 4.4 and $BW$ is the total bandwidth of all the transmitted pulses combined. Given a system with three antennas, a bandwidth of about 640 MHz, and a carrier frequency ($f_c$) of 9.6 GHz, the resulting transmitted waveforms in the frequency domain are shown in Figure 1 for a single pulse.

The frequency spectrum plot highlights the orthogonality of the chosen waveforms. It also brings to light some topics that will be discussed further in the following sections. First, a full resolution SAR image can be formed by coherently summing the backprojection images formed for each individual channel. Second, since each MISO channel has a reduced bandwidth compared to the traditional SIMO approach, the STAP resolution is reduced by a factor of the number of transmit antennas. There are additional considerations for the MISO STAP model that will arise during the system model derivations and are discussed in-depth later.

## 3. MISO SAR SYSTEM MODEL

Given the orthogonal FDMA signal model in the previous section, it is possible to separate each transmit channel at the receiver. Backprojection can then be done for each of the separated channels, forming lower down-range resolution images. By coherrently summing the backprojected images from each channel, a full resolution SAR image is formed.[1]

## 4. MISO STAP PROCESSING

Although the SAR system model extensions for this scheme are straightforward, greater detail needs to be provided for the MISO STAP model. We will begin by defining the system model and show intermittent steps that follow the derivation of our modified STAP model. We follow the derivations originally given by Ward[2] for the single transmit, multiple receive (SIMO) case, highlighting departures from the traditional SIMO case. After completion of the derivation, the final steering vectors for this model will be given. The steering vector definitions are important as it will be shown that this scheme will require full matched filtering to perform STAP.

### 4.1 System Model

The system model derivation follows that of Ward with modifications for this FMDA scheme. First, the definition of a received signal for a single target for one antenna is

$$\bar{s}_{n,m}(t) = a_r u(t-\tau_n)\exp\{2\pi(f_c + f_{n,m} + f_{t,n})(t-\tau_n)\}\exp\{j\psi\} \tag{3}$$

where $a_r$ is the echo amplitude and

$$f_{t,n} = \frac{2v_t}{\lambda_n} \tag{4}$$

is the target's Doppler frequency. From this point forward, we will drop the subscript $m$ from the notation for simplicity although the frequency $f_n$ and any variable containing it, will vary as a function of antenna and pulse number. In this definition, $v_t$ is the radial velocity of the target and $\lambda_n = c/(f_c + f_n)$. Next, the delay $\tau_n$ consists of two parts,

$$\tau_n = \tau_t + \tau'_n \tag{5}$$

where $\tau_t = (2R_t)/c$, the round trip delay to the target, and $\tau'_n$ is the delay to each of the antennas relative to the reference antenna. The relative delay to each antenna is then calculated as

$$\tau'_n = -n\frac{d}{c}\cos\theta_t \sin\phi_t \tag{6}$$

where d is the spacing between antennas, and $\theta_t$ and $\phi_t$ are the angles to the target as given in the model setup by Ward. Using this definition it is then possible to define a spatial frequency as

$$\vartheta_{t,n} = \frac{d}{\lambda_n}\cos\theta_t \sin\phi_t \tag{7}$$

so then the phase delay to the $n^{th}$ antenna is

$$-\omega_n \tau'_n = n2\pi\vartheta_{t,n} \ . \tag{8}$$

Now assuming that the waveforms are narrowband, the relative delay term is not significant within the complex envelope of the signal. With this assumption, the signal model can then be simplified to

$$\bar{s}_n(t) = a_r \exp\{j\psi\}\exp\{jn2\pi\vartheta_t\}u(t-\tau_t)\exp\{j2\pi f_t t\}\exp\{j2\pi(f_c+f_n)t\}\exp\{-j2\pi f_n \tau_t\} \tag{9}$$

and some of the remaining phase terms are absorbed into the phase term $\psi$. Finally, down-converting the signal to baseband

$$s_n(t) = \bar{s}_n(t)\exp\{-j2\pi(f_c+f_n)t\} \tag{10}$$

which results in

$$s_n(t) = a_r \exp\{j\psi\}\exp\{jn2\pi\vartheta_{t,n}\}u(t-\tau_t)\exp\{j2\pi f_{t,n} t\}\exp\{-j2\pi f_n \tau_t\} \ . \tag{11}$$

The rest of the derivation follows the steps in Ward with the only difference being the term $\exp\{-j2\pi f_n \tau_t\}$. This exponential term is a range dependent phase wrap. It is because of this term that full matched filters must be used instead of fast Fourier transforms; thus, the computational complexity of the proposed scheme is higher than that of the traditional approach.

### 4.2 Steering Vectors

The rest of the system model derivation follows the steps presented by Ward. These steps have already been shown in Bryant[1] and Ward[2] and can be referenced there. The final data stored from a single target is

$$x_{nm} = \alpha_t \exp\{jn2\pi\vartheta_{t,n}\}\exp\{jm2\pi\bar{\omega}_{t,n}\}\exp\{-j2\pi f_n \tau_t\} \tag{12}$$

where $\alpha_t = a_r \exp\{j\psi\}$ is the complex random amplitude, $\bar{\omega}_{t,n} = f_{t,n}/f_r$ is the normalized Doppler frequency and $f_r$ is the pulse repetition frequency. Then for a given coherent processing interval (CPI), $x_{nm}$ is an $N \times M$ matrix where $N$ is the number of antennas and $M$ is the number of pulses.

It can be seen that the matrix $x_{nm}$ can be separated into spatial and temporal parts as a function of $n$ and $m$ respectively. These separated vectors are referred to as spatial and temporal steering vectors. Their individual definitions are not presented here as the focus will be on the single space-time steering vector which is a combination of the two. The definitions of the separate steering vectors can be found in Bryant.[1] The

space-time steering vector will be noted by $\mathbf{v}(\vartheta, \bar{\omega})$ and is an $NM \times 1$ vector which is formed by stacking the columns of $x_{nm}$ on each other. The return from a target can then be simply written as

$$\mathbf{y}_t = \alpha_t \mathbf{v}(\vartheta_{t,n}, \bar{\omega}_{t,n}) \ . \tag{13}$$

Then if $\mathbf{y}$ is a sum of space-time steering vectors from various targets, the angle/velocity matched filter response of the targets can be found by

$$z = \mathbf{v}(\vartheta, \bar{\omega})^H \mathbf{y} \tag{14}$$

varying $\vartheta$ and $\bar{\omega}$ over possible test values.

### 4.3 System Drawbacks

As previously noted, this system has larger range bins for STAP as a result of the decreased bandwidth of the transmitted pulses. Additionally, the range dependent phase wrap that comes about from the different carrier frequencies for each transmitter does not allow the data to be processed using fast Fourier transforms. Instead, the computational complexity is increased since there is need to implement full matched filters. Finally, coherence on clutter is not maintained using a fixed subcarrier frequency at each antenna; lack of coherence would render STAP wholly ineffective. Indeed, Rabideau[3] shows that the fixed, non-scheduled FDMA scheme is not the best choice of orthogonal waveforms as it does not have the required MISO cancellation ratio (MCR) for clutter cancellation. Despite the bleak outlook for this system, we show in the following section that it is still possible to maintain coherence on clutter by scheduling the assignment of subcarrier frequencies to each antenna as a function of pulse number.

### 4.4 Waveform Scheduling

To overcome the problem of losing coherence on clutter as a function of the distance between the sub-band carriers, we propose a waveform schedule. By defining the variable $I_{n,m}$ as a function of $n$, $m$, and a variable $\beta$, it is possible to maintain coherence on clutter. Note that $\beta$ is defined as the number of half inter-element spacings the radar platform travels between pulses, or

$$\beta = \frac{2v_a}{d \times f_r}, \tag{15}$$

where $v_a$ is the along-track speed of the platform and $d$ is the distance between antennas in the uniform linear array (ULA). Now that $\beta$ has been defined we propose a scheme for scheduling the waveforms to maintain clutter coherence. To accomplish this, we will define $I_{n,m}$ as

$$I_{n,m} = 1 + (n + \lfloor m\beta \rfloor) \bmod N \quad n = 0, 1, ..., N-1, \quad m = 1, 2, ..., M-1 \ , \tag{16}$$

and for $m = 0$, the first pulse, $I_{n,0} = n + 1$. Here, $\lfloor x \rfloor$ denotes largest integer not greater than $x$. For the case that $\beta = 1$ it can be shown that the coherence of the clutter can be maintained by rotating which carrier frequency is transmitted from each antenna at each pulse. Figure 2 helps to illustrate this idea. When the clutter is coherent, it causes the clutter covariance matrix to have a reduced rank. This is one way in which we can use the simulation below to determine the effectiveness of this waveform scheduling.

## 5. MISO FDMA SIMULATION

To simulate this proposed FDMA MISO scheme, a wide-area simulation is written in MATLAB (Mathworks, Natick, MA). This section discusses the set-up of the simulation as well as the results. The simulation generates returned signals for scatterers modeling clutter and combines them all at the receiver. The signals are then separated back into separate transmit channels using mixing at the different sub-band frequencies and low pass filtering. This process is repeated for each pulse in a given coherent processing interval and the results are stored. This entire process is repeated for different realizations of clutter so that an estimated covariance matrix can be generated. This estimated clutter covariance matrix is then used to calculate performance metrics that quantify the effectiveness of the proposed FDMA MISO scheme.

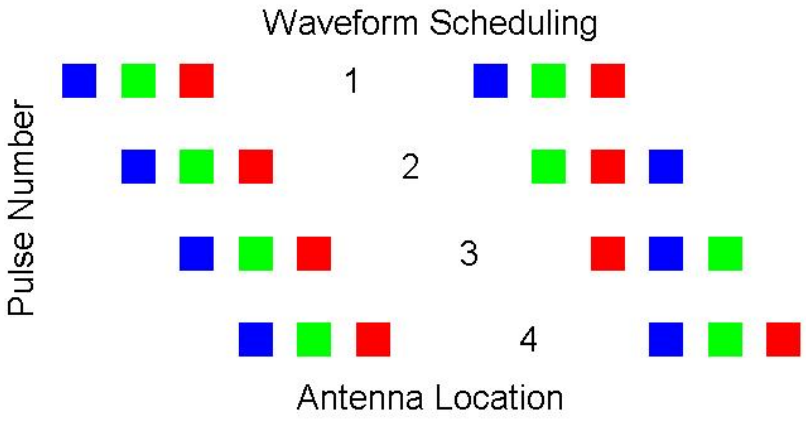


Figure 2: Example of waveform scheduling for integer $\beta$. Left: fixed subcarrier frequencies without scheduling. Right: scheduled FDMA waveforms.

### 5.1 Methods

To simulate clutter, multiple point scatterers are used within a given range cell, each with the same radar cross section (RCS). The point scatterers are randomly distributed in angle and also range. Although the range is randomly distributed, it is limited to within a single resolution cell; this allows the simulation to run only for one range under test. The delays to each scatterer are calculated and the received waveforms are generated for each transmitted waveform. Since all of the scatterers have the same RCS, the reflectivity of the returned pulse is a function of the antenna gain. A Gaussian beam pattern is used in these simulations. The received waveforms are then summed to simulate the single receiver. The individual channels are then separated at the receiver by mixing down the received signal to the various basebands and filtering. The final separated receive signal is then stored and the simulation is run again for a different realization of the clutter. This is repeated for $5MN$ realizations.[4]

The covariance matrix is then estimated using Equation 17

$$\hat{\Sigma} = \frac{1}{L}\sum_{l=1}^{L} \mathbf{y}_l^* \mathbf{y}_l^T \tag{17}$$

where $L = 5MN$, $*$ denotes conjugation, and $\mathbf{y}_l$ is the vectorized data for the $l^{th}$ realization of the clutter. This estimated covariance matrix is used to calculate various performance metrics.

The three metrics that will be focused on here are clutter covariance rank, adapted pattern, and minimum detectable velocity (MDV). The simulation only calculates the returns for 10 pulses; this size of CPI is not typical in practice (more pulses would be used for finer velocity resolution) but it is enough so that the performance can be observed while keeping computation time practical. The results of the simulation are presented in the following subsection.

### 5.2 Results

The simulation is run for three settings. Two cases consider integer $\beta$: once without the proposed waveform scheduling and again with the proposed scheduling. The third trial will test the non-integer $\beta$ case using waveform scheduling. Once the phase history for every realization of the clutter is saved, they are then loaded and used to form an estimated clutter covariance matrix. The rank of the clutter covariance is then observed to see if clutter coherence has been retained. A low-rank indicates that there is coherence. For the integer $\beta$ case, it has

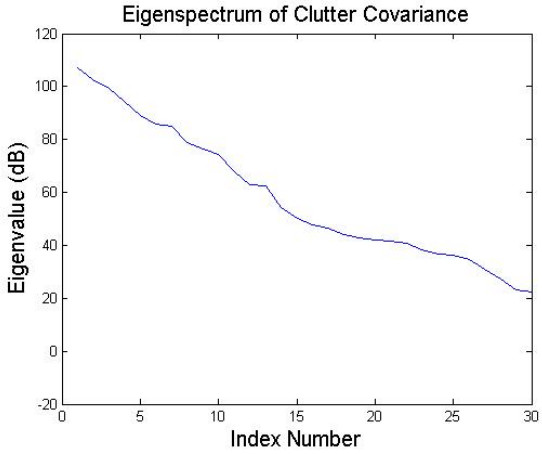


(a) Eigenspectrum of clutter covariance for non-rotating scheme.

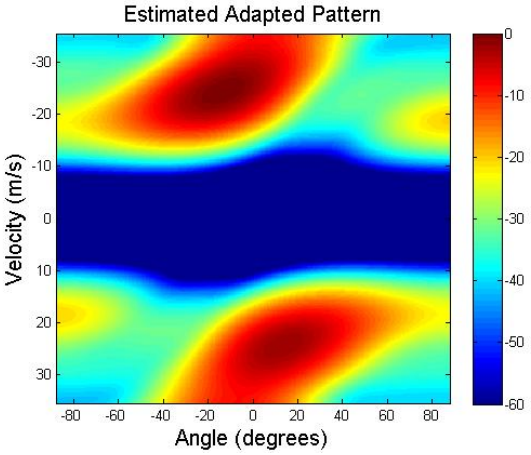


(b) Adapted pattern for non-rotating scheme.

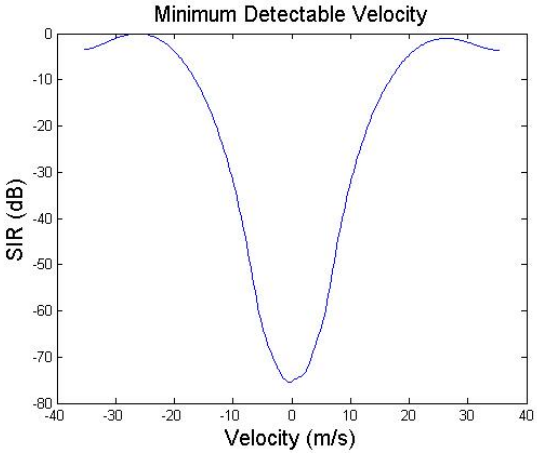


(c) MDV for non-rotating scheme.

Figure 3: Simulated results for the non-scheduled (non-rotating) scheme

been shown that the waveform scheduling approach should produce a covariance matrix with a rank that can be calculated using Brennan's Rule.[1,2] Additionally, the covariance matrix of the non-scheduled scheme is expected to be full rank. The results of the non-scheduled scheme are now given and discussed.

The first result of the non-scheduled scheme is the rank of the clutter covariance matrix. This is shown in Figure 3a which is a plot of the sorted Eigenvalues of the clutter covariance matrix. This plot confirms that the covariance matrix has a full rank as expected, with no clear break in eigenvalues. Next, the adapted pattern shows the clutter cancellation ability of the scheme. An ideal adapted pattern would have deep and narrow nulls in the angle and velocity regions that coincide with clutter returns, leaving the rest of the region available for target detection. As Rabideau[3] has already shown mathematically, the FDMA non-scheduled scheme is unable to maintain coherence on the clutter, and this is seen by the large area suppressed in the adapted pattern in Figure 3b. Finally, the MDV is used to check the ability of the system to null clutter. The MDV statistic is essentially a vertical cut through the adapted pattern at a given angle. Therefore, an ideal MDV plot would have a deep null corresponding to the velocity of the clutter that is induced by the velocity of the platform at the given angle. For simplicity, the MDV is calculated at an angle of zeros degrees so that the clutter will have a zero velocity. Figure 3c shows that this scheme cannot null clutter effectively made apparent by the wide null across a large range of velocities. All of these results confirm what has already been shown by Rabideau;[3] a fixed FDMA scheme is a poor choice for MISO STAP systems. These results will be used to compare against the success of our proposed FDMA waveform scheduled scheme.

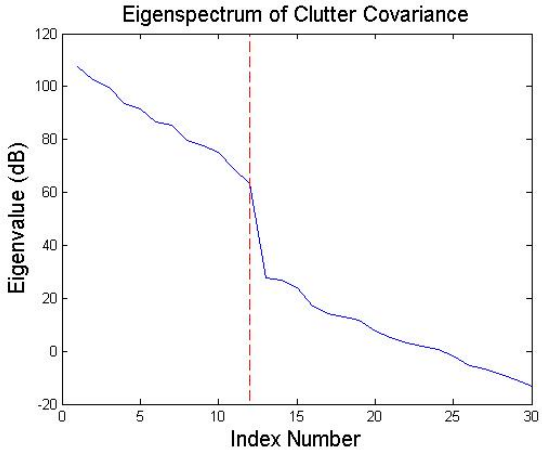


(a) Eigenspectrum of clutter covariance for rotating scheme.

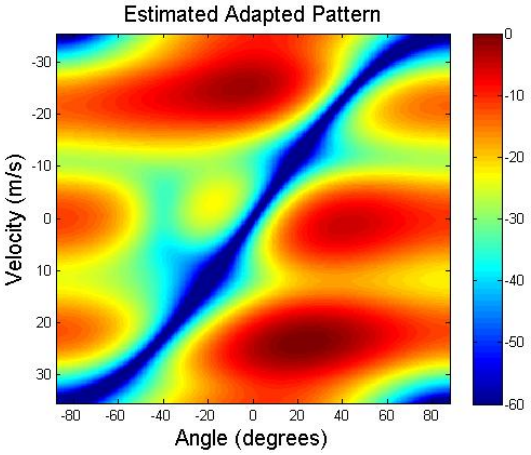


(b) Adapted pattern for rotating scheme.

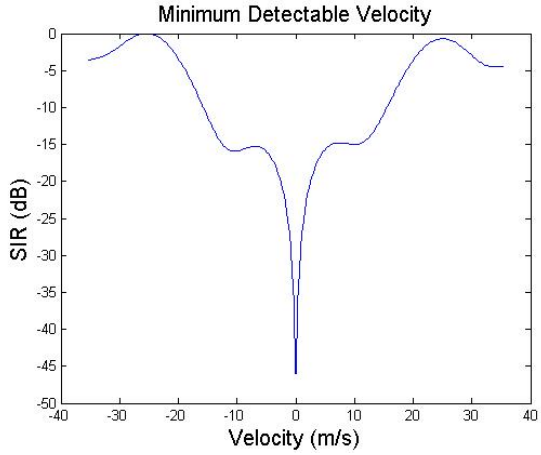


(c) MDV for rotating scheme.

Figure 4: Simulated results for the scheduled (rotating) scheme

The same metrics are again calculated, this time for the waveform scheduled case, still with an integer $\beta$. The rank of the clutter covariance matrix is shown in Figure 4a. The dotted line shows the rank predicted by Brennan's Rule. As desired, the waveform scheduling scheme maintains the low rank property of the clutter covariance matrix and matches Brennan's Rule. Next, the adapted pattern for this approach is compared to the previous non-scheduled scheme. It is clear from observing Figure 4b that this waveform scheduled approach is much better at canceling clutter. This is evidenced by the nulling that takes place only over the curve where the clutter is expected to lie. For the $\beta = 1$ case, the clutter is expected to lie on a line that takes a 45 degree angle across the angle/velocity plot. The null observed here is curved because the results are plotted as a function of the angle and not the sine of the angle. The final metric is again the MDV. It can be seen in Figure 4c that the nulling only occurs at zero velocity as expected. These results help to illustrate that this FDMA waveform scheduled scheme can maintain coherence on clutter and provide the adaptive nulling required for STAP.

Comparing the results of the non-scheduled sheme to the waveform scheduled scheme, it is clear that the introduction of the waveform scheduling as a function of $\beta$ and pulse number allows for adaptive clutter nulling. These are promising results but it has so far only been shown to work for the case when $\beta$ is an integer. We will now show results of the simulation run for a non-integer $\beta$ case using the waveform scheduling with a hold-to-rotate approach in Equation 16. It can be seen from Figure 5a and Figure 5b that the proposed waveform schedulling scheme still works for a non-integer $\beta$.

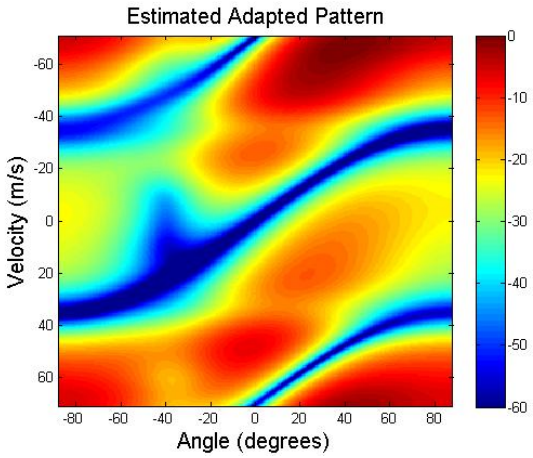


(a) Adapted pattern for rotating scheme ($\beta = \frac{1}{2}$).

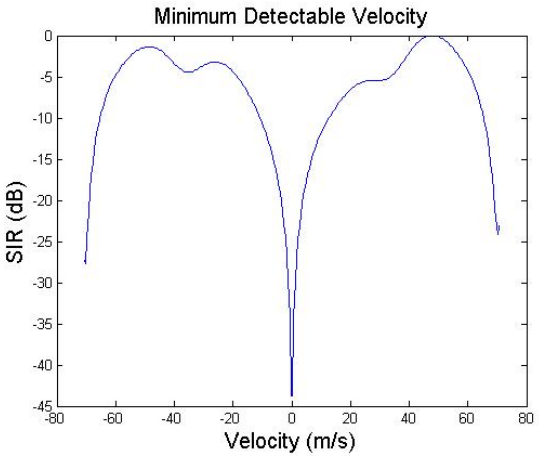


(b) MDV for rotating scheme ($\beta = \frac{1}{2}$).

Figure 5: Simulated results for scheduled waveform scheme, non-integer $\beta$

## 6. CONCLUSION

We have proposed a MISO radar model that uses orthogonal FDMA waveforms to provide the degrees of freedom required to perform space time adaptive processing while constraining the data-rate of the system to that of a single receive channel. It is shown that this scheme can maintain full resolution SAR imagery by coherently summing the backprojection images from each of the channels. Additionally, STAP can be performed using the provided degrees of freedom with small model extensions. This MISO STAP is shown to have an increase in computational complexity since FFTs cannot be used and has coarser downrange resolution by a factor of the number of transmit antennas. We also introduce a waveform scheduling idea that allows the system to maintain clutter coherence so that effective clutter cancellation can be achieved. Given this final FDMA MISO model, a MATLAB simulation is created and run to test the performance of the scheme. The results of the simulation confirm that the system is able to maintain coherence on clutter, thus enabling effective clutter nulling that makes space time adaptive processing useful.

## 7. ACKNOWLEDGEMENTS

We would like to thank Steve Scarborough and Dr. Michael Minardi for their insight that prompted this exploration. This work was supported by industrial and government membership fees to the Center for Surveillance Research, a National Science Foundation I/UCRC.

## REFERENCES

1. C. Bryant, E. Ertin, and L. C. Potter, "Combining synthetic aperture radar and space-time adaptive processing using a single receive channel," pp. 80510G–80510G–14, 2011.
2. J. Ward, *Space-time Adaptive Processing for Airborne Radar*, Technical report (Lincoln Laboratory), Massachusetts Institute of Technology, Lincoln Laboratory, 1994.
3. D. Rabideau, "Doppler-offset waveforms for mimo radar," in *Radar Conference (RADAR), 2011 IEEE*, pp. 965–970, 2011.
4. M. Richards, *Fundamentals of Radar Signal Processing*, McGraw-Hill Electronic Engineering Series, McGraw-Hill Education, 2005.